Electronic Supplementary Material (ESI) for Energy & Environmental Science.

Electronic Supporting Information

Platinum(II)-porphyrin as a photosensitizer for visible light-driven water oxidation in neutral phosphate buffer solution

Hung-Cheng Chen,[a] Dennis G. H. Hetterscheid,[a,b] René M. Williams,[a] Jarl Ivar van der Vlugt,[a] Joost N. H. Reek,*[a] Albert M. Brouwer*[a]

[a] *Van 't Hoff Institute for Molecular Sciences, University of Amsterdam, P.O. Box 94157, 1090 GD Amsterdam, The Netherlands. E-mail: A.M.Brouwer@uva.nl*

[b] *present address: Faculty of Science, Leiden Institute of Chemistry, Einsteinweg 55, P.O. Box 2333 CC Leiden, The Netherlands.*

Experimental Section

Electrochemical measurements: The electrochemical measurements were performed with a potentiostat/galvanostat MacLab model ML160 controlled by resident software (E-chem v 1.5.2 for Windows) using a conventional single-compartment three-electrode cell with a platinum working electrode, a silver wire as reference electrode, and a platinum wire as counter electrode. All measurements in dichloromethane were carried out with freshly distilled solvent with a solute concentration of ca. 1.0 mM in the presence of tetraethylammonium hexafluorophosphate, NBu_4PF_6 (0.1 M) as supporting electrolyte and a scan rate of 100 mV s^{-1}. Ferrocene was added at the end of the experiment as internal standard. For the aqueous cyclic voltammetry measurements, a three-electrode cell setup was used with glassy carbon working electrode, platinum wire counter electrode and Ag/AgCl, 3 M KCl reference electrode. NaH_2PO_4/Na_2HPO_4 (0.2 M, pH = 7.0) was the supporting electrolyte.

Photophysical measurements: UV/Vis absorption spectra were measured on a Shimadzu UV-2700 spectrophotometer using 10 mm path-length quartz cuvettes. Emission spectra were measured on a Spex Fluorolog 3 spectrometer, equipped with double grating monochromators in the excitation and emission channels. The excitation light source was a 450 W Xe lamp and the detector a Peltier cooled R636-10 (Hamamatsu) photomultiplier tube. The emission spectra were corrected for the wavelength response of the detection system. Time resolved emission measurements were measured using a Hamamatsu streak camera (ref. S1) and a Coherent Infinity laser for excitation.

Light-driven oxygen evolution measurements: the oxygen evolution was analyzed by a Clark-type oxygen electrode (Hansatech Instruments, DW2/2 unit with an S1 electrode). A 120 W halogen lamp was used as the illumination light source. In other experiments a 532 nm green laser (Changchun New Industries, CNI model with PSU-H-LED) was used. The laser power was varied, and was measured using a power meter (Coherent). The reaction vessel was cooled with flowing water adjusted to T = 20 °C. The signal was calibrated using air saturated aqueous solutions ($[O_2]$ = 276.3 μM, T = 20 °C) and N_2-purged solutions ($[O_2] \approx 0$). Before each measurement, the mixture was also purged with N_2 to provide an oxygen-free solution. In order to confirm the oxygen generation coming from light driven water oxidation, the illumination starts after ~2 minutes of flat zero $[O_2]$ signal in dark. The maximum turnover frequency (TOF_{max}) was determined at the steepest slope of the oxygen evolution curve. The turnover number was determined by the ratio of the mole number of O_2 related to mole number of catalyst at a given time.

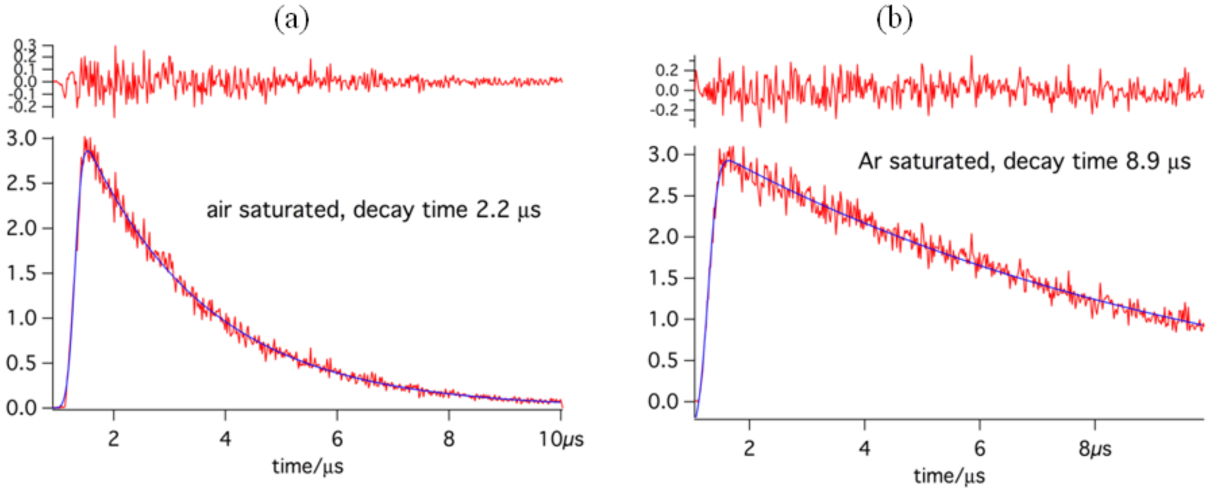

Figure S1. Phosphorescence decays of Pt(II)-TCPP (1.1 × 10^{-4} M) in (a) air saturated and (b) Ar-purged pH 7.0, 0.1 M phosphate buffer solutions upon excitation with 2 ns pulses at 532 nm. The decays were fitted with a single-exponential decay function convolved with a Gaussian Instrument Response Function.

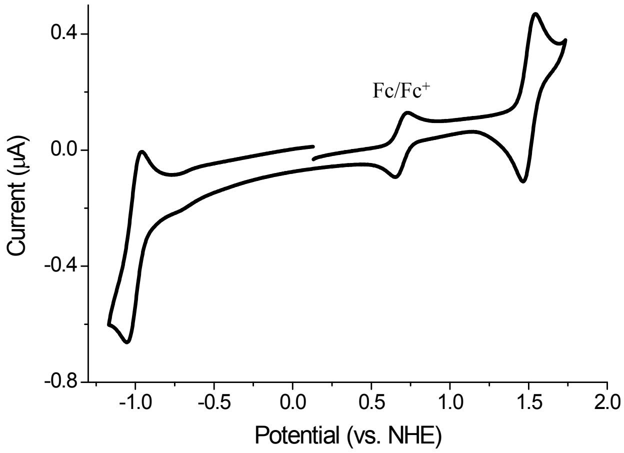

Figure S2. Cyclic voltammograms of Pt(II)-TCMePP (1 mM) in CH_2Cl_2 solution with 0.1 M TBAP electrolyte. Fc/Fc^+ used as internal standard, and NHE = Fc/Fc^+ + 0.69 V.

The redox potentials were measured relative to Fc/Fc^+. For this standard, $E_{1/2}(Fc/Fc^+) = 0.475$ V vs SCE in dichloromethane. Hence, $E_{1/2}(Pt^{III/II}) = 1.285$ V vs. SCE which is very close to the value reported in ref. S11.

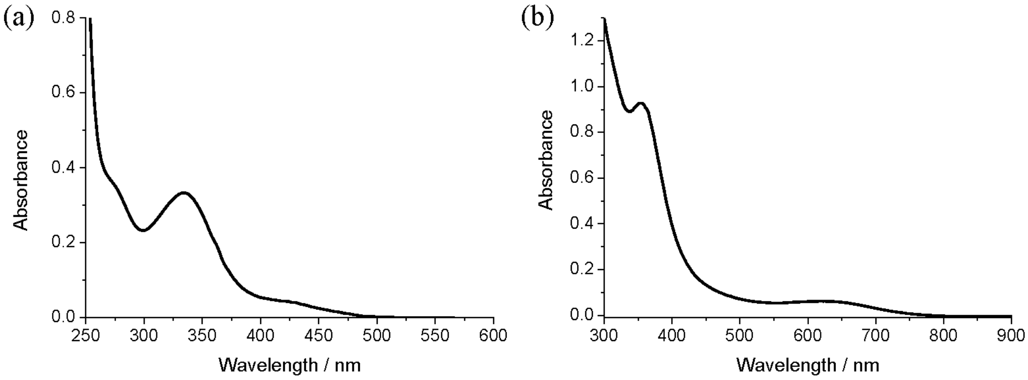

Figure S3. Absorption spectra of (a) Ir-NHC complex (10^{-4} M) (b) Co_4O_4-cubane (1.7×10^{-4} M) in phosphate buffer (pH = 7.0, 0.1 M) in a 1-cm path length cell.

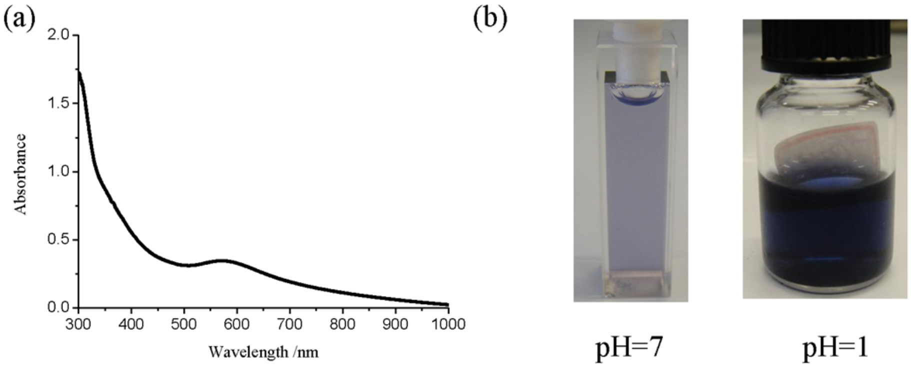

Figure S4.(a) absorption spectrum of $IrO_x \cdot nH_2O$ nanoparticles in pH = 7 solution (b) pictures of solutions of $IrO_x \cdot nH_2O$ nanoparticles at pH = 7 (left) and at pH = 1 (right).

Control experiments for light-driven water oxidation

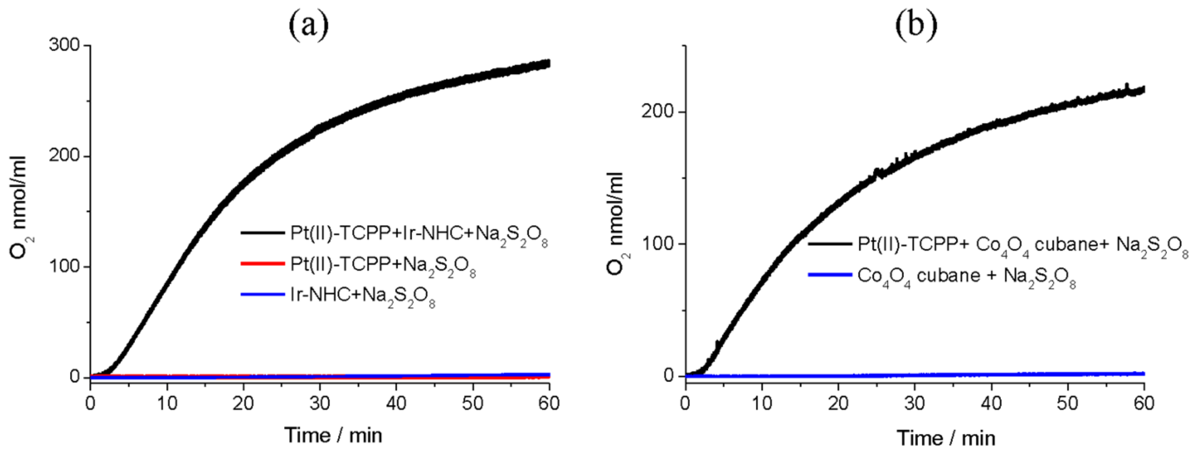

Figure S5. (a) Photochemical oxygen evolution in 1.5 mL of a pH 7.0, 0.1 M phosphate buffer solution containing $Na_2S_2O_8$ (5.0×10^{-2} M), Pt(II)-TCPP (6.7×10^{-4} M) and catalysts : (a) Ir-NHC (5.0×10^{-5} M), (b) Co_4O_4 cubane (5.0×10^{-5} M). The red line is the control experiment without catalyst, Ir-NHC. The blue lines are the control experiments without Pt(II)-TCPP.

Photocatalytic reaction with $Ru(bpy)_3^{2+}$ in phosphate buffer solution

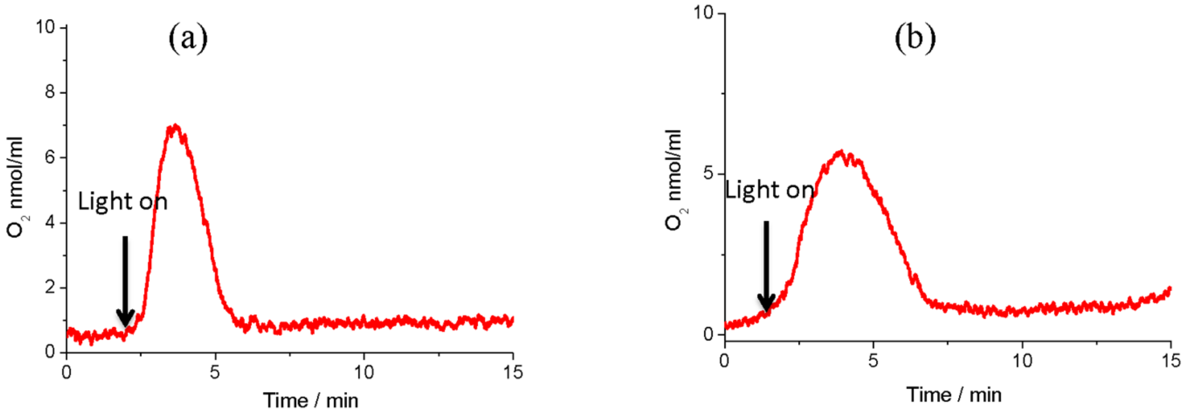

Figure S6. (a) Photochemical oxygen evolution in 1.5 mL of a pH 7.0, 0.1 M phosphate buffer solution containing $Na_2S_2O_8$ (5.0×10^{-2} M), $Ru(bpy)_3^{2+}$ (6.7×10^{-4} M) and catalysts : (a) Ir-NHC (5.0×10^{-5} M), (b) Co_4O_4 cubane (5.0×10^{-5} M).

Determination of the maximum turnover frequency TOF$_{max}$ under 120 W halogen lamp excitation

Here, the maximum turnover frequency TOF$_{max}$ are calculated under the assumption that the catalysts stay intact during the water oxidation.

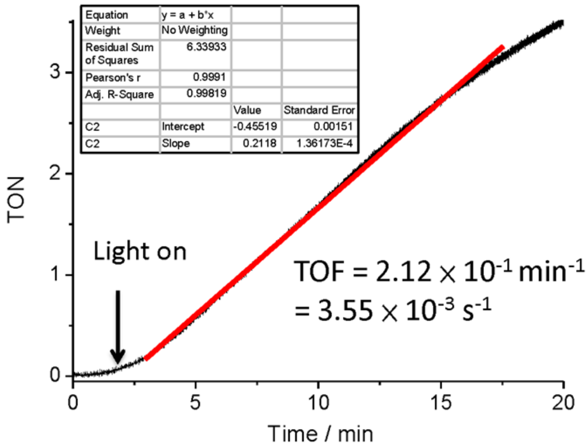

Equation	y = a + b*x		
Weight	No Weighting		
Residual Sum of Squares	6.33933		
Pearson's r	0.9991		
Adj. R-Square	0.99819		
		Value	Standard Error
C2	Intercept	-0.45519	0.00151
C2	Slope	0.2118	1.36173E-4

Figure S7. The determination of TOF by linear fitting of O_2 generation. The 1.5 mL of phosphate buffer solution contains $Na_2S_2O_8$ (5.0 × 10^{-2} M), Pt (II)-TCPP (6.7 × 10^{-4} M) and Ir-NHC (5.0 × 10^{-5} M).

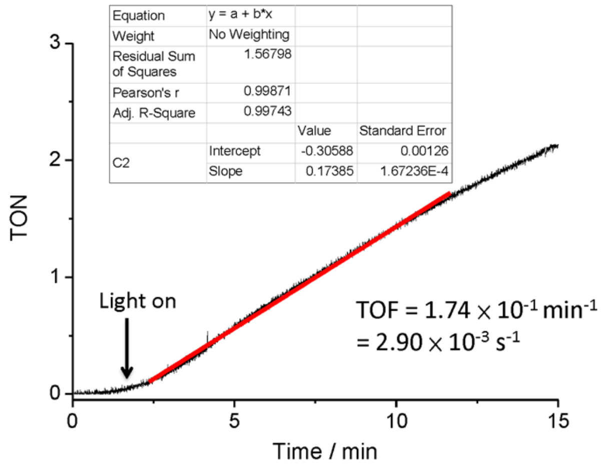

Equation	y = a + b*x		
Weight	No Weighting		
Residual Sum of Squares	1.56798		
Pearson's r	0.99871		
Adj. R-Square	0.99743		
		Value	Standard Error
C2	Intercept	-0.30588	0.00126
	Slope	0.17385	1.67236E-4

Figure S8. The determination of TOF by linear fitting of O_2 generation. The 1.5 mL of phosphate buffer solution contains $Na_2S_2O_8$ (5.0 × 10^{-2} M), Pt (II)-TCPP (6.7 × 10^{-4} M) and Co_4O_4-cubane (5.0 × 10^{-5} M).

For Ir-NHC, the maximum turnover frequency TOF$_{max}$ of the catalyst was observed to be 3.6 × 10^{-3} mol O_2 (mol of Ir-NHC)$^{-1}$ s^{-1}.

For Co_4O_4-cubane, the TOF$_{max}$ = 2.9 × 10^{-3} mol O_2 (mol of Co_4O_4-cubane)$^{-1}$ s^{-1} was obtained. Noticeably, our TOF$_{max}$ is about one order of magnitude smaller than reported in ref. S5.

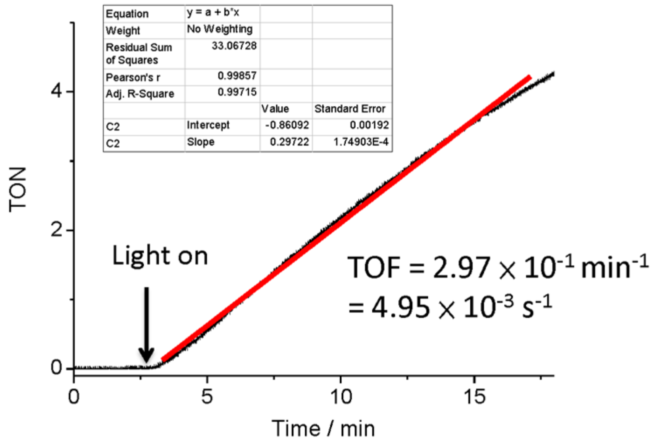

Figure S9. The determination of TOF by linear fitting of O_2 generation. The 1.5 mL of phosphate buffer solution contains $Na_2S_2O_8$ (5.0×10^{-2} M), Pt (II)-TCPP (6.7×10^{-4} M) and $IrO_x \cdot nH_2O$ nanoparticles (1.8×10^{-4} M).

For the $IrO_x \cdot nH_2O$ nanoparticles, the $TOF_{max} = 5 \times 10^{-3}$ mol O_2 (mol of Ir atom)$^{-1}$ s^{-1} was obtained assuming that that 20% of the Ir atoms are on the surface of ligand-free 2 nm diameter $IrO_x \cdot nH_2O$ nanoparticles. Our TOF_{max} of $IrO_x \cdot nH_2O$ nanoparticles is about one order of magnitude smaller than that reported in ref. S12 or ref. S13. Their TOF = 4.9×10^{-2} mol O_2 (mol of Ir atom)$^{-1}$ s^{-1} was obtained with succinate stabilized 2 nm diameter $IrO_x \cdot nH_2O$ nanoparticles in pH 5.8 $Na_2SiF_6/NaHCO_3$ buffer. Interestingly, the rate of our system is one order of magnitude higher than reported in ref. S14 or ref. S13. Their TOF = 4.0×10^{-4} mol O_2 (mol of Ir atom)$^{-1}$s^{-1} was obtained from $IrO_x \cdot nH_2O$ nanoparticles at pH 5.0.

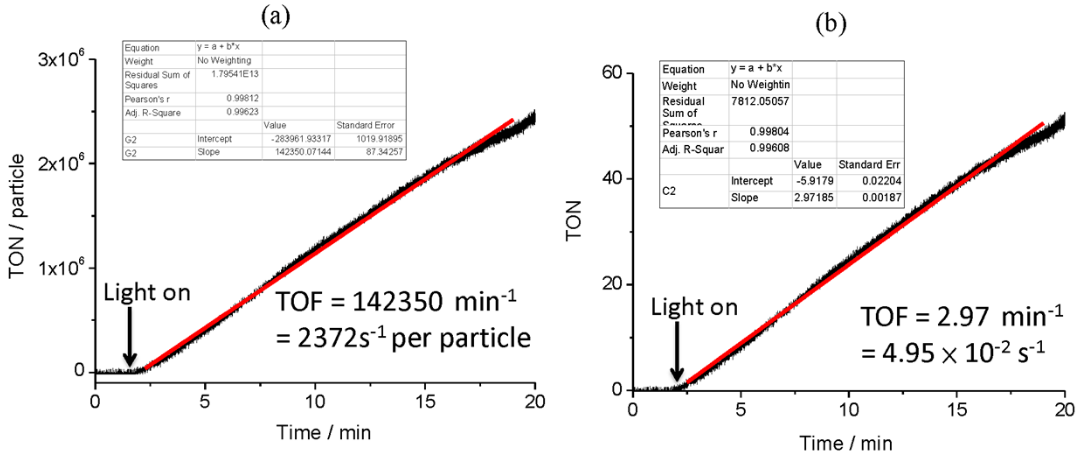

Figure S10. The determination of TOF by linear fitting of O_2 generation. The 1.5 mL of phosphate buffer solution contains $Na_2S_2O_8$ (5.0×10^{-2} M), Pt (II)-TCPP (6.7×10^{-4} M) and Co_3O_4 nanoparticles (4.16×10^{-5} g/ml = 4.17×10^{10} particles = 6.93×10^{-5} nmol). Calculated in (a) is the TOF by per nanoparticle and (b) is the TOF by per active Co atom on surface.

According to ref. S2, the unit cell edge lengths are 8.084 Å for Co_3O_4 nanoparticles, thus the density of surface cobalt atoms is 6.1×10^{18} surface cobalt atoms/m^2. The average number of active Co atoms on the surface of 50 nm diameter Co_3O_4 nanoparticles is estimated to be 4.8 ×

10^4. TOF_{max}= 2372 s^{-1} per particle was obtained. This leads to a TOF_{max}= 4.9 × 10^{-2} mol O_2 (mol of Co atom)$^{-1}$ s^{-1} and TOF_{max}= 0.29 s^{-1} nm^{-2} of surface area. Compared to other light-driven water oxidation systems that used Co_3O_4 nanoparticles as catalyst, our TOF value is of the same order of magnitude. Frei et al. (ref. S10 and ref. S15) found TOF = 1 × 10^{-2} s^{-1} per surface Co center of SBA-15/Co_3O_4 (4 wt%) and TOF = 1 s^{-1} nm^{-2} of projected surface area with the Na_2SiF_6-$NaHCO_3$ buffer system (22 mM, pH = 5.8).

Photostability tests

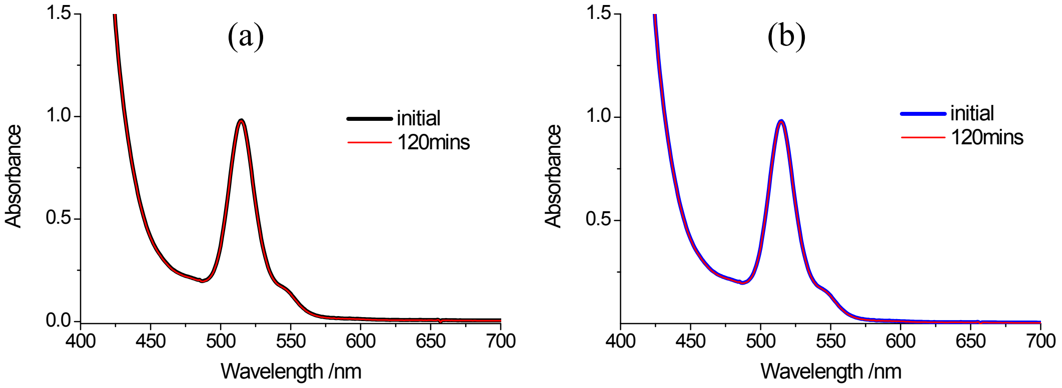

Figure S11. Absorption spectrum of Pt(II)-TCPP (6.7 × 10^{-4} M) in pH 7.0, 0.1 M phosphate buffer solutions before irradiation and after 120 minutes under halogen lamp irradiation. (a) air saturated (b) degassed condition. A 1 mm path length cuvette was used.

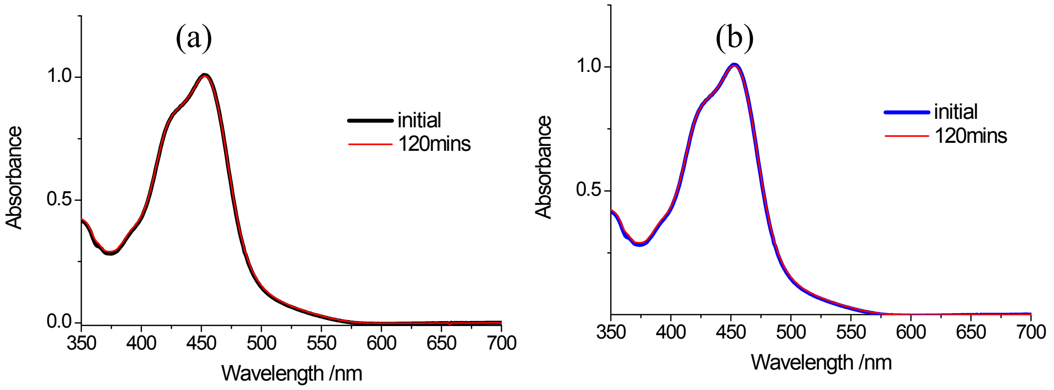

Figure S12. Absorption spectrum of $Ru(bpy)_3^{2+}$ (6.7 × 10^{-4} M) in pH 7.0, 0.1 M phosphate buffer solutions before irradiation and after 120 minutes under halogen lamp irradiation. (a) air saturated (b) degassed condition. A 1 mm path length cuvette was used.

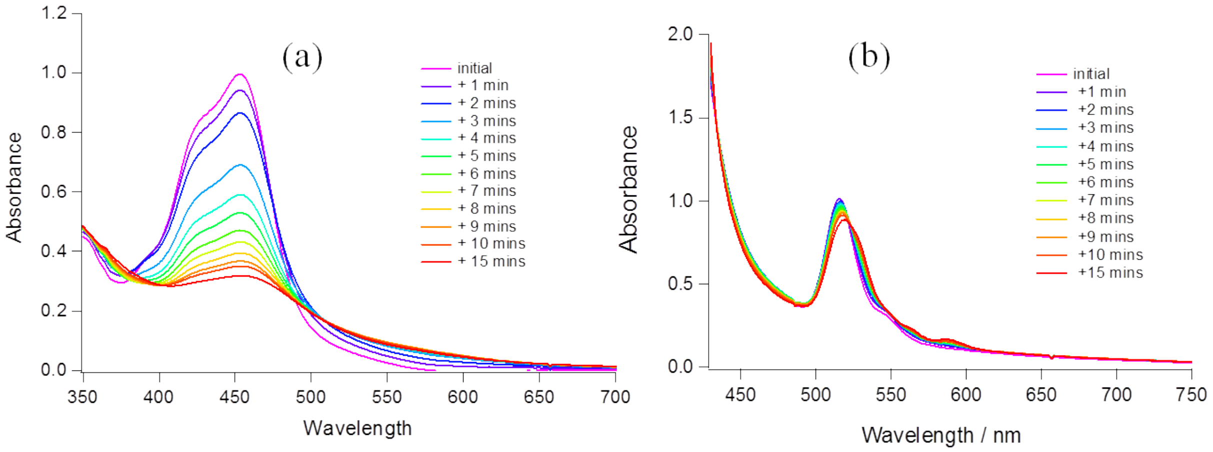

Figure S13. Absorption spectra of (a) $Ru(bpy)_3^{2+}$ (6.7×10^{-4} M), (b) Pt(II)-TCPP (6.7×10^{-4} M) with Ir-NHC (5.0×10^{-5} M) and $Na_2S_2O_8$ (5.0×10^{-2} M) in pH 7.0, 0.1 M phosphate buffer solutions as a function of time under halogen lamp illumination. A 1 mm path length cuvette was used.

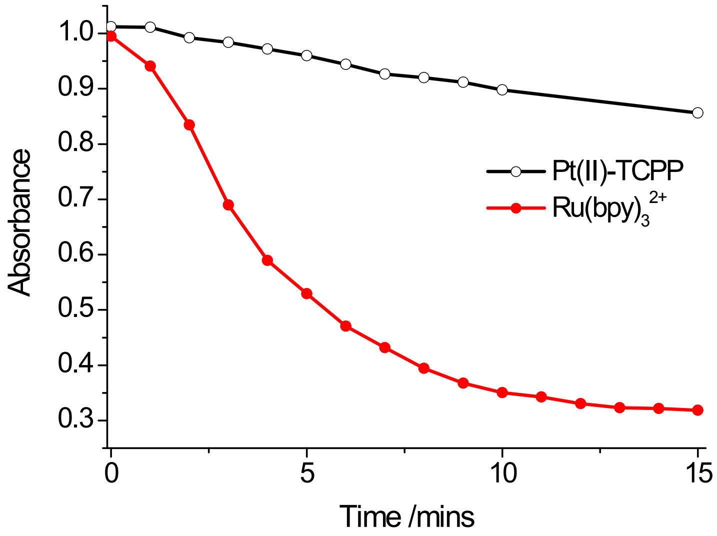

Figure S14. Absorbance changes as a function of irradiation time for $Ru(bpy)_3^{2+}$ (at 452 nm) and for Pt(II)-TCPP (515 nm) in figure S13.

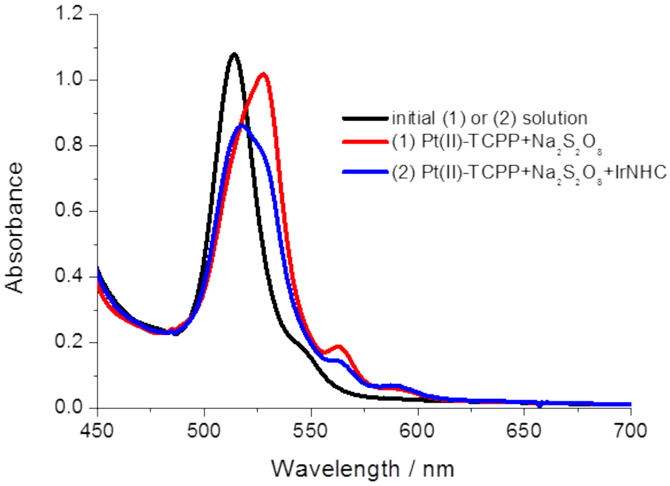

Figure S15. Absorption spectra before and after irradiation of phosphate buffer solutions of (1) Pt(II)-TCPP (6.7 × 10^{-5} M) and $Na_2S_2O_8$ (1.7 × 10^{-2} M), and (2) Pt(II)-TCPP, $Na_2S_2O_8$ and Ir-NHC (3.3 × 10^{-5} M. Photodegradation is clearly less in the presence of the WOC. A 1 mm path length cuvette was used.

Rate of bimolecular electron transfer to persulfate

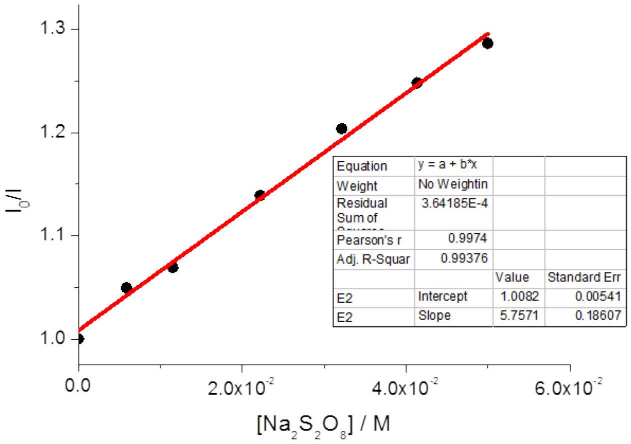

Equation	y = a + b*x		
Weight	No Weightin		
Residual Sum of	3.64185E-4		
Pearson's r	0.9974		
Adj. R-Squar	0.99376		
		Value	Standard Err
E2	Intercept	1.0082	0.00541
E2	Slope	5.7571	0.18607

Figure S16. Plot of I_0/I against [$Na_2S_2O_8$] for the emission quenching of Pt(II)-TCPP in pH 7.0 phosphate buffer solutions at air saturated condition (I_0 is the emission intensity in the absence of $Na_2S_2O_8$; I is the emission intensity in the presence of $Na_2S_2O_8$).

When there is only bimolecular dynamic quenching in an emission system, we can use the following Stern-Volmer equation:

$I_0/I = 1 + \tau_0 k_q [Q]$

Here, k_q is the bimolecular quenching constant and τ_0 is the Pt-TCPP emission lifetime in the absence of quencher. In air-saturated solution, we found $\tau_0 = 2.2$ μs. Hence, the bimolecular quenching constant of Pt(II)-TCPP with $Na_2S_2O_8$ is $k_q = 2.6 \times 10^6$ $M^{-1}s^{-1}$.

From the triplet lifetimes of Pt-TCPP in air-saturated and Ar-saturated solutions (Figure S1), we can deduce the energy transfer rate to oxygen $k_{et} = 3.4 \times 10^5$ s^{-1} in air saturated condition. With the bimolecular quenching constant $k_q = 2.6 \times 10^6$ $M^{-1}s^{-1}$ and the quencher concentration

$[Na_2S_2O_8] = 5.0 \times 10^{-2}$ M, the quenching rate by electron transfer $k_q \times [Na_2S_2O_8] = 1.3 \times 10^5\ s^{-1}$ can be deduced. Consequently, the electron transfer rate with $Na_2S_2O_8$ is of the same order as the triplet-triplet energy transfer between ^{3}Pt-TCPP and $^3O_2$ in air saturated condition.

Determination of the maximum turnover frequency TOF_{max} under 532 nm laser excitation with different irradiation powers

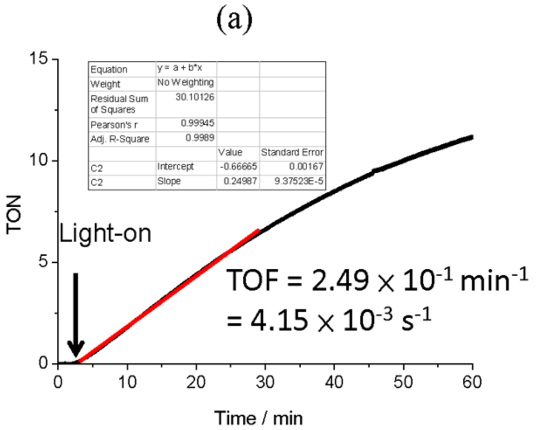

Equation	y = a + b*x		
Weight	No Weighting		
Residual Sum of Squares	30.10126		
Pearson's r	0.99945		
Adj. R-Square	0.9989		
		Value	Standard Error
C2	Intercept	-0.66665	0.00167
C2	Slope	0.24987	9.37523E-5

Equation	y = a + b*x		
Weight	No Weighting		
Residual Sum of Squares	70.96558		
Pearson's r	0.99909		
Adj. R-Square	0.99819		
		Value	Standard Error
F2	Intercept	-0.83201	0.0026
F2	Slope	0.29054	1.38918E-4

Figure S17. The determination of TOF under excitation power density of 532 nm laser of (a) 5.2 mW and (b) 21.2 mW by linear fitting of O_2 generation. The 1.5 mL of phosphate buffer solution contains $Na_2S_2O_8$ (1.67×10^{-2} M), Pt (II)-TCPP (2.23×10^{-4} M) and Ir-NHC (1.67×10^{-5} M).

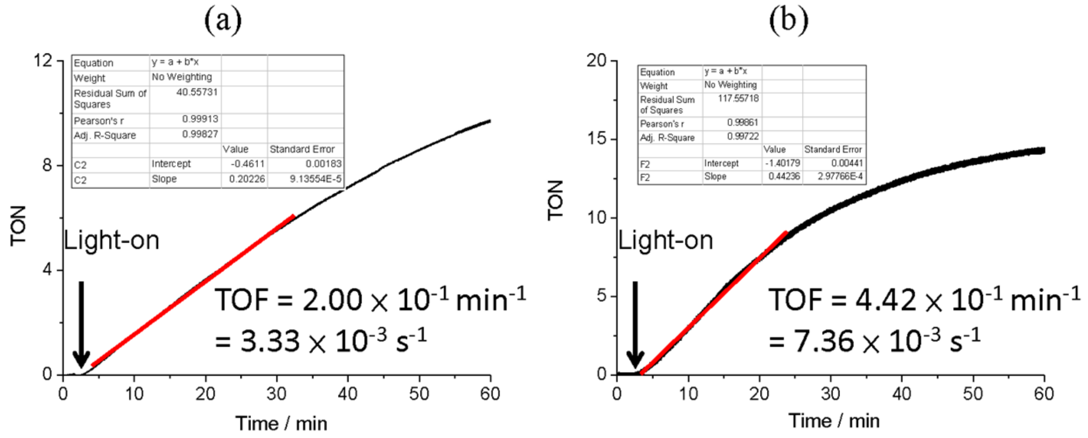

Equation	y = a + b*x		
Weight	No Weighting		
Residual Sum of Squares	40.55731		
Pearson's r	0.99913		
Adj. R-Square	0.99827		
		Value	Standard Error
C2	Intercept	-0.4611	0.00183
C2	Slope	0.20226	9.13554E-5

Equation	y = a + b*x		
Weight	No Weighting		
Residual Sum of Squares	117.55718		
Pearson's r	0.99861		
Adj. R-Square	0.99722		
		Value	Standard Error
F2	Intercept	-1.40179	0.00441
F2	Slope	0.44236	2.97766E-4

Figure S18. The determination of TOF under excitation power density of 532 nm laser with (a) is 5.2 mW and (b) 21.2 mW by linear fitting of O_2 generation. The 1.5 ml of phosphate buffer solution contains $Na_2S_2O_8$ (1.67×10^{-2} M), Pt (II)-TCPP (2.23×10^{-4} M) and Co_4O_4-cubane (1.67×10^{-5} M).

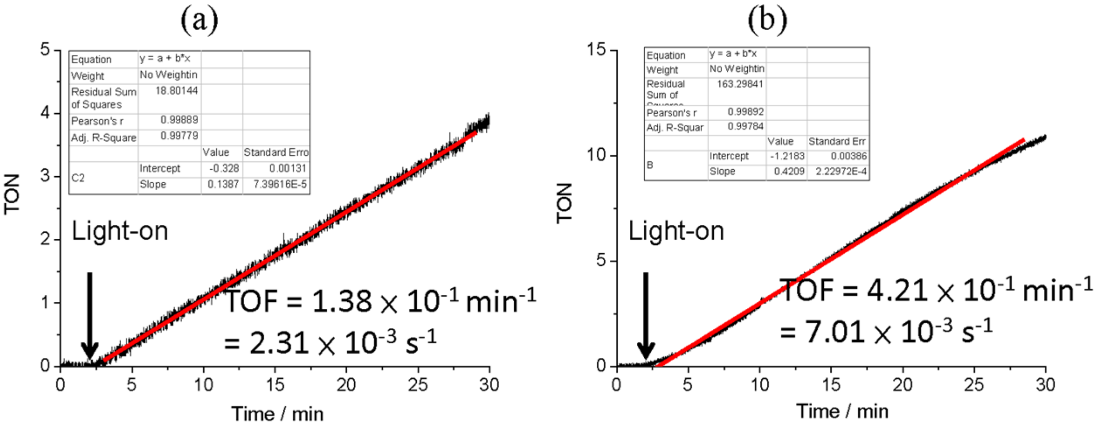

Figure S19. The determination of TOF under excitation power density of 532 nm laser of (a) 5.2 mW and (b) 51.6 mW by linear fitting of O_2 generation. The 1.5 mL of phosphate buffer solution contains $Na_2S_2O_8$ (1.67×10^{-2} M), Pt (II)-TCPP (2.23×10^{-4} M) and $IrO_x \cdot nH_2O$ nanoparticles (6.0×10^{-5} M).

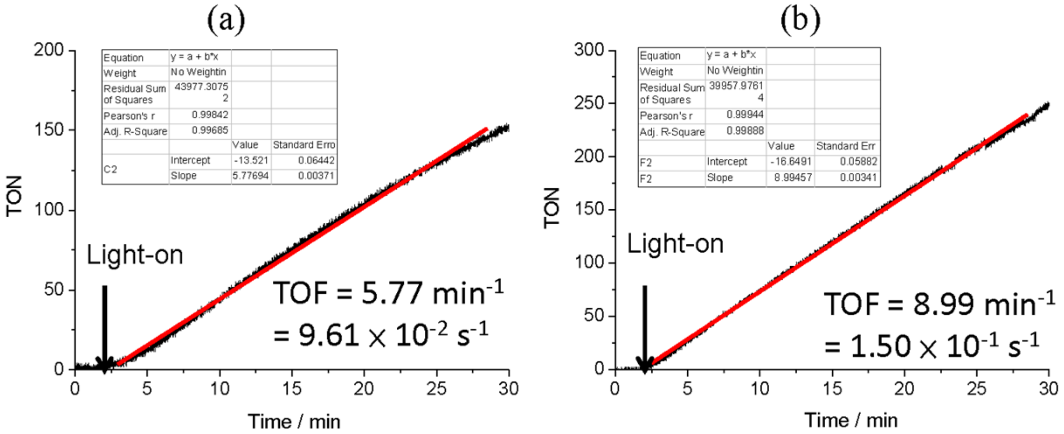

Figure S20. The determination of TOF under excitation power density of 532 nm laser of (a) 5.2 mW and (b) 21.2 mW by linear fitting of O_2 generation. The 1.5 mL of phosphate buffer solution contains $Na_2S_2O_8$ (1.67×10^{-2} M), Pt(II)-TCPP (2.23×10^{-4} M) and Co_3O_4 nanoparticles (1.39×10^{-5} g/ml = 1.04×10^{10} particles = 1.73×10^{-5} nmol).

Quantum yield determination under 532 nm laser excitation

The net light-driven water oxidation reaction with Pt(II)-TCPP as photosensitizer and persulfate as sacrificial electron acceptor is expressed below :

$$\mathrm{PtTCPP^{4-} + h\nu \longrightarrow PtTCPP^{4-*}}$$

$$\mathrm{PtTCPP^{4-*} + S_2O_8^{2-} \longrightarrow PtTCPP^{\bullet 3-} + SO_4^{\bullet -} + SO_4^{2-}}$$

$$\mathrm{PtTCPP^{4-} + SO_4^{\bullet -} \longrightarrow PtTCPP^{\bullet 3-} + SO_4^{2-}}$$

$$\mathrm{4PtTCPP^{\bullet 3-} + 2H_2O \xrightarrow{WOC} O_2 + 4H^+ + 4PtTCPP}$$

$$\mathrm{2S_2O_8^{2-} + 2H_2O + 2h\nu \longrightarrow O_2 + 4H^+ + 4SO_4^{2-}}$$

The quantum yield of water oxidation by photons $\Phi(H_2O)$ is two times the number of moles of oxygen produced divided by the number of moles of photons absorbed by the Pt(II)-TCPP in the total illumination time.

The photon flux corresponding to 5.2 mW of 532 nm green laser is equal to 2.31×10^{-8} einstein/s. There is ~4% reflection loss at the glass/air interface and the transmission of borosilicate glass reaction vessel is ~90% at 532 nm. Hence the incident photon flux is ~2.0×10^{-8} einstein/s.

The molar absorptivity of Pt(II)-TCPP at 532 nm is 3846 M^{-1} cm^{-1}, [Pt-TCPP] is 2.23×10^{-4} M and the light path length in the reaction vessel is 1 cm. According to the Lambert-Beer law, the number of moles of photons absorbed by the Pt(II)-TCPP is then ~1.7×10^{-8} einstein/s. The quantum yield of water oxidation was calculated by 30 minutes total irradiation time.

WOCs	$[O_2]$ nmol/ml at 30 mins	reaction volume /ml	illumination time /s	O_2 mol	Total photons absorbed by PtTCPP /einstein	$\Phi(H_2O)$ / %
Ir-NHC	121	1.5	1800	1.82E-07	3.10E-05	1.17
Co_4O_4 cubane	110	1.5	1800	1.65E-07	3.10E-05	1.07
$IrO_x \cdot nH_2O$	61	1.5	1800	9.18E-08	3.10E-05	0.59
Co_3O_4	65	1.5	1800	9.75E-08	3.10E-05	0.63

Synthesis and sample preparation:

Pt(II) meso-tetra(4-methoxycarbonylphenyl)porphyrin Pt(II)-TCMePP; Pt(II) meso-tetra(4-carboxyphenyl)porphyrin Pt(II)-TCPP

Both for Pt(II)-TCMePP and Pt(II)-TCPP the synthesis procedures were followed according to ref. S3.

Iridium-N-Heterocyclic carbene complex; Ir-NHC

The synthesis procedures can be found in ref. S4.

Co_4O_4 cubane complex; $Co_4O_4(OAc)_4(py)_4$:

The synthesis procedure followed the method of ref. S5.

$IrO_x \cdot nH_2O$ nanoparticles in phosphate buffer (pH = 7.0, 0.1 M) solution

The synthesis procedures of ref. S6 were followed. We took 5 mL acidic $IrO_x \cdot nH_2O$ nanoparticles stock solution and then adjusted to desired pH 7 by addition of dilute 1 M NaOH solution. The 1 mL neutral $IrO_x \cdot nH_2O$ nanoparticles solution was added into 1 mL phosphate buffer (pH = 7.0, 0.2 M) solution. Finally, get the $IrO_x \cdot nH_2O$ nanoparticles in phosphate buffer (pH =7.0, 0.1 M) solution. The concentration of $IrO_x \cdot nH_2O$ nanoparticles was evaluated using the extinction coefficient of 630 L mol^{-1} cm^{-1} at 574 nm from ref. S6.

Co_3O_4 nanoparticles in phosphate buffer (pH = 7.0, 0.1 M) solution

We directly suspended 5 mg of the black Co_3O_4 nanopowder < 50 nm particle size [Sigma-Aldrich, CAS number: 1308-06-1] into 40 mL phosphate buffer (pH = 7.0, 0.1 M) solution. The stock Co_3O_4 nanoparticle solution (1.25×10^{-4} g/mL) was sonicated for 2 hr before it was used for the light-driven water oxidation study.

References

S1. X. Y. Lauteslager, I. H. M. van Stokkum, H. J. van Ramesdonk, A. M. Brouwer, and J. W. Verhoeven, *J. Phys. Chem. A*, 1999, **103**, 653–659.

S2. A. J. Esswein, M. J. McMurdo, P. N. Ross, A. T. Bell, and T. D. Tilley, *J. Phys. Chem. C*, 2009, **113**, 15068–15072.

S3. R. P. Briñas, T. Troxler, R. M. Hochstrasser, and S. A. Vinogradov, *J. Am. Chem. Soc.*, 2005, **127**, 11851–11862.

S4. D. G. H. Hetterscheid and J. N. H. Reek, *Chem. Commun.*, 2011, **47**, 2712–2714.

S5. N. S. McCool, D. M. Robinson, J. E. Sheats, and G. C. Dismukes, *J. Am. Chem. Soc.*, 2011, **133**, 11446–11449.

S6. Y. Zhao, E. A. Hernandez-Pagan, N. M. Vargas-Barbosa, J. L. Dysart, and T. E. Mallouk, *J. Phys. Chem. Lett.*, 2011, **2**, 402–406.

S7. S. Berardi, G. La Ganga, M. Natali, I. Bazzan, F. Puntoriero, A. Sartorel, F. Scandola, S. Campagna, and M. Bonchio, *J. Am. Chem. Soc.*, 2012, **134**, 11104–11107.

S8. P. G. Hoertz, Y.-I. Kim, W. J. Youngblood, and T. E. Mallouk, *J. Phys. Chem. B*, 2007, **111**, 6845–6856.

S9. A. Harriman, I. J. Pickering, J. M. Thomas, and P. A. Christensen, *J. Chem. Soc., Faraday Trans. 1.*, 1988, **84**, 2795–2806.

S10. F. Jiao and H. Frei, *Angew. Chem. Int. Ed.*, 2009, **48**, 1841–1844.

S11. P. Chen, O. S. Finikova, Z. Ou, S. A. Vinogradov, and K. M. Kadish, *Inorg. Chem.*, 2012, **51**, 6200–6210.

S12. P. G. Hoertz, Y.-I. Kim, W. J. Youngblood, and T. E. Mallouk, *J. Phys. Chem. B*, 2007, **111**, 6845–6856.

S13. J. R. Swierk and T. E. Mallouk, *Chem. Soc. Rev.*, 2013, **42**, 2357–2387.

S14. A. Harriman, I. J. Pickering, J. M. Thomas, and P. A. Christensen, *J. Chem. Soc., Faraday Trans. 1.*, 1988, **84**, 2795–2806

S15. F. Jiao and H. Frei, *Energy Environ. Sci.*, 2010, **3**, 1018–1027.